ICAS-98-7,7,2

A98-31711

# A FINITE ELEMENT STUDY OF THE POSTBUCKLING BEHAVIOUR OF A FLAT STIFFENED PANEL

C J Lynch*, S G Sterling**

Department of Aeronautical Engineering
The Queen's University of Belfast

## Abstract

Analytical methods currently used to determine the buckling/postbuckling behaviour of aircraft fuselage structures are based on empirical/semi-empirical data and are hence over-conservative. The finite element (FE) method has the potential to eliminate this conservatism. A finite element study of the buckling and postbuckling behaviour of a flat stiffened riveted panel subjected to uniform in-plane compression is presented. The element type and mesh density required to accurately predict the buckling mode is investigated. Various methods of modelling the skin/stringer interface are also investigated and the importance of correctly modelling the behaviour in this region highlighted. Results from the FE analyses are compared to both experimental data and theoretical predictions. Correlation between FE predictions and test data is seen to be very good, the FE buckling and failure loads being within 2.5% of the experimental values. The theoretical predictions are used to demonstrate the range of conservatism associated with current analytical techniques. Results indicate a possible weight reduction of 5-12% by employing the FE technique over conventional analytical methods.

## Introduction

Stiffened panels can be designed to efficiently support in-plane compression, bending and shear loads and hence, are the basic building blocks of most aircraft fuselage structures. As the buckling skin arrangement offers notable weight savings over the non-buckling skin, these structures are frequently designed to buckle at load levels significantly lower than the limit load. Thus the determination of the buckling loads, post-buckling behaviour and failure loads is essential for the design of these structures.

Methods currently employed to determine this information typically involve design formulae (many of which are outlined by Bruhn[1] ) based on empirical/semi-empirical data. These formulae were developed mainly to deal with plate or column instabilities and hence their extension to deal with the buckling/post-buckling behaviour of stiffened panels requires dividing the panels into a series of plates and columns. Hence assumptions must be made regarding the support offered by the stiffeners to the skin, the effective width and length of pre-buckled skin panels between stiffeners and the effective width of post-buckled skin acting with the stiffeners, to list some of the main factors. Due to these assumptions, the calculations possess an inherent conservatism which inevitably leads to over-designed structures. This conservatism could potentially be eliminated through the use of non-linear post-buckling finite element analyses which have not, as yet, been fully exploited.

A great deal of research has been carried out over the past couple of decades on the application of the FE technique to structural instability. Over recent years much of this work has focused on composite structures[2-7] while there has been relatively little research concerning FE postbuckling analysis of conventional isotropic structures. This is primarily due to the lack of alternative analytical tools to reliably predict the buckling/postbuckling behaviour of composite structures and the existence of equivalent tools to predict the corresponding behaviour in isotropic structures, despite the conservatism associated with these tools.

Percy[8] analysed a Ti-6-4 hat stiffened panel subjected to both uniform compression and temperature gradients using the FE technique and obtained good correlation between the predicted and experimentally observed pre- and postbuckling behaviour. The FE buckling loads were within 7% of the corresponding test results although no comparison was made for the failure loads and failure modes. FE predictions of the buckling loads of this panel subjected to uniform compression and uniform shear (without temperature gradients) were presented by Ko and Jackson [9,10]. The difference between the FE and experimental buckling loads was around 4% for the case of uniform compression, however experimental data was not available for uniform shear loading. The failure loads of two mild-steel uniformly compressed blade stiffened panels were determined both

* Postgraduate Research Student
** Senior Lecturer

experimentally and numerically by Shanmugam and Arockiasamy[11]. The FE failure loads were 7% and 15% higher than the experimentally observed values for each panel.

These results highlight the improved accuracy of the FE technique in determining the buckling loads of complicated structural configurations and also the need for a better understanding of the factors influencing the failure of these structures. This paper presents a finite element methodology for the postbuckling analysis of a typical riveted aircraft fuselage panel subjected to uniform in-plane compression loading. The analyses were carried out using the commercial FE code ABAQUS[12]. Several factors relating to the nonlinear FE analysis of shell structures will be considered. The mesh density required to accurately capture the buckling modes for different element types will be determined. Different methods of modelling the skin/stringer interface will also be considered and the resulting load-deflection characteristics for each model will be compared to both experimentally obtained data and theoretical predictions to determine the optimum modelling technique. Finally the panel will be redesigned (assuming MIL-HDBK[13] material properties) to carry prescribed design loads using both the FE method and the conventional theoretical technique. The resulting panel geometries will be used to estimate the potential weight savings achievable.

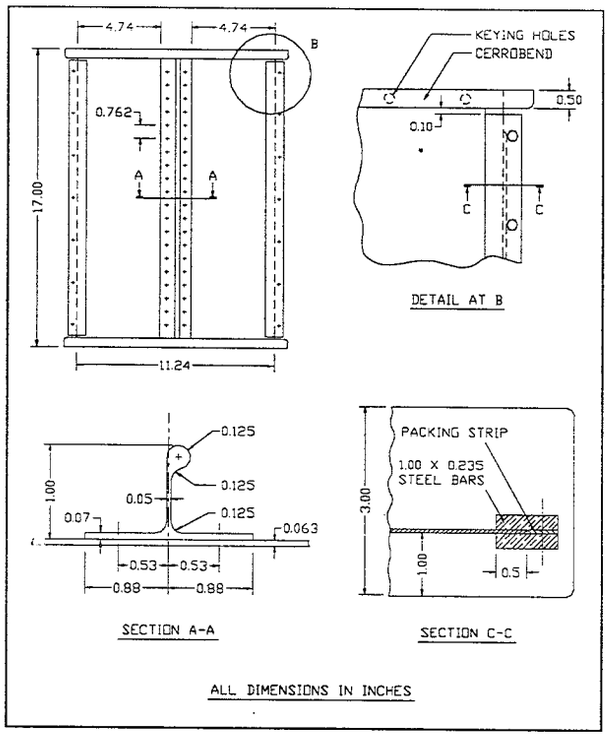


Figure 1: Test Panel Dimensions

## Experimental Investigation

### Test Panel Details

The panel considered consisted of a 11.24"×17" flat skin stiffened by a bulbed-tee stringer, as shown in Figure 1. The skin material was 2024-T3 clad aluminium alloy and the stringer 2024-T3511 aluminium alloy extrusion, heat treated to the T8511 temper. The skin was cut in such a way that its grain (longitudinal) direction lined up with the stringer which was then fastened to the skin by two rows of 5/32" diameter MS20426 countersunk rivets. The ends of the assembled panel were potted in Cerrobend low melting point alloy and machined flat and parallel in a direction perpendicular to the skin. Support conditions at the unloaded edges of the skin were similar to those used by Rothwell[14] and are outlined in Figure 1. A clearance of 0.2" was provided between the Cerrobend and the support bars to ensure that the compressive load would be solely carried by the skin and stringer.

### Test Procedure

The panel was tested in a 25t capacity hydraulic, displacement-controlled, compression testing machine. Relative motion between the two platens was measured using two linear voltage displacement transducers (LVDT's) located close to the edges of the panel. The panel was also extensively strain-gauged although the resulting strain distributions will not be presented in this paper. The strain gauge, LVDT and load information were recorded via a Spectra-DAS data logging system which scanned at approximately 4 second intervals. Before any load had been applied to the panel the strain gauges were zeroed. A small load of about 100lbf was then applied and final adjustments made to ensure that the panel was perpendicular to the platens. The LVDT's were also zeroed at this stage. The load was then applied at a rate of approximately 2500 lbf/min until failure occurred.

| | 2024-T3 | |
|---|---|---|
| | Test data | MIL-HDBK |
| E (Psi) | $9.576\times10^6$ | $10.70\times10^6$ |
| m | 9.7 | 13 |
| $f_n$ (Psi) | 36714 | 33110 |
| $f_{cy}$ (Psi) | 43400 | 39000 |
| $\nu$ | 0.33 | 0.33 |
| | 2024-T8511 | |
| | Test data | MIL-HDBK |
| E (Psi) | $10.857\times10^6$ | $11.00\times10^6$ |
| m | 24.2 | 16[a] |
| $f_n$ (Psi) | 62841 | 50485[b] |
| $f_{cy}$ (Psi) | 68600 | 57000 |
| $\nu$ | 0.33 | 0.33 |

(a) As m was not available for 2024-T8511, the 2024-T3511 value was assumed

(b) This value was calculated (based on a Ramberg-Osgood fit) using $f_{cy}$ and the assumed m value

Table 1: Material properties used in analyses

Material Tests

Prior to the analysis compression tests were carried out to determine the skin and stringer material properties. For each material three specimens were tested and the results averaged over the three specimens. These test specimens were cut from the same batch of material as the skin and stringer of the test panel. The results from these tests together with the MIL-HDBK compression values are given in Table 1.

## Finite Element Modelling

Element Choice

Several different elements in ABAQUS were examined to determine their suitability for buckling analysis of shell structures. The characteristics of these elements are outlined in Table 2. All elements are curved shells and use five degrees of freedom per node except for S4R which uses six degrees of freedom per node. A more detailed description of these elements can be found in the ABAQUS Theory Manual[15].

| Element type | Geometry | Characteristics |
|---|---|---|
| S8R5 | quadrilateral | second-order 8-noded small strain thin shell with reduced integration |
| S4R5 | quadrilateral | first-order 4-noded small strain thin shell with reduced integration |
| S4R | quadrilateral | first-order 4-noded finite strain general purpose shell with reduced integration |
| STRI65 | triangular | second-order 6-noded small strain thin shell |
| STRI35 | triangular | first-order 3-noded small strain thin shell |

Table 2: Shell element characteristics

These elements were used to model a simply supported flat plate subjected to uniform longitudinal compression. The plate had a length $a = 6"$, width $b = 6"$ and thickness $t = 0.063"$ with Young's modulus, $E = 11.0\times10^6$ Psi. Eigenvalue buckling analyses were performed to determine the mode1 and mode2 buckling stresses. The performance of each element was then assessed based on the convergence (with increasing mesh density) of these buckling stresses to the corresponding theoretical values, given by the following equation:

$$f_b = \frac{k\pi^2 E}{12\left(1-\nu^2\right)}\left(\frac{t}{b}\right)^2 \qquad (1)$$

where $k$ is the buckling coefficient and $\nu = 0.33$ is Poisson's ratio. The first buckling mode consists of one half-wavelength along the plate (in the direction of the loading) and one half-wavelength across the plate whereas the second mode consists of two half-wavelengths along the plate and one half-wavelength across the plate, giving corresponding buckling coefficients of 4 and 6.25 and buckling loads of 4477lbf and 6996lbf respectively. The results of this mesh convergence study are given in Figures 2 and 3. It is evident that S8R5 and STRI35 elements provide more accurate solutions than the other elements for relatively coarse meshes although STRI35 is a constant strain element and hence is liable to be overstiff. It is also worth noting that both 4-noded quadrilateral elements require a finer mesh to obtain the same level of accuracy as S8R5, STRI35 and STRI65 elements which converge to within 1% of the theoretical model buckling stress with nine nodes along either edge of the plate. It was decided, based on these findings, to model the skin, stringer flange and stringer web using S8R5 elements with approximately four elements (nine nodes) per buckle half-wavelength and to model the bulb with three-noded quadratic beam elements B32.

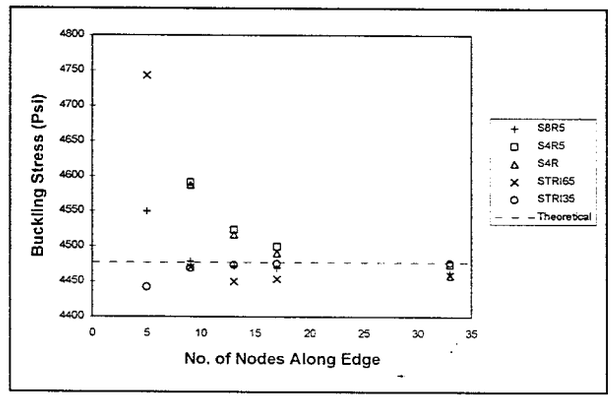


Figure 2: Convergence of buckling stresses with increasing mesh density for model

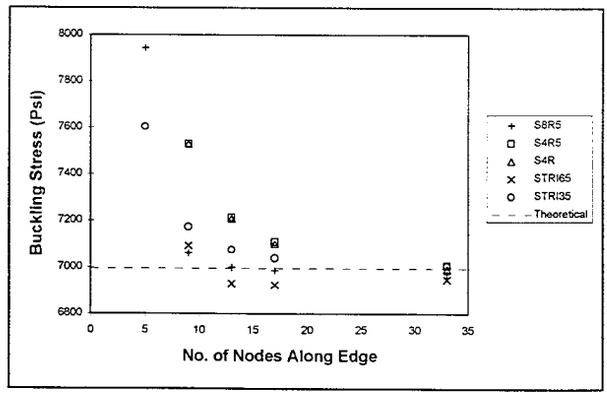


Figure 3: Convergence of buckling stresses with increasing mesh density for mode2

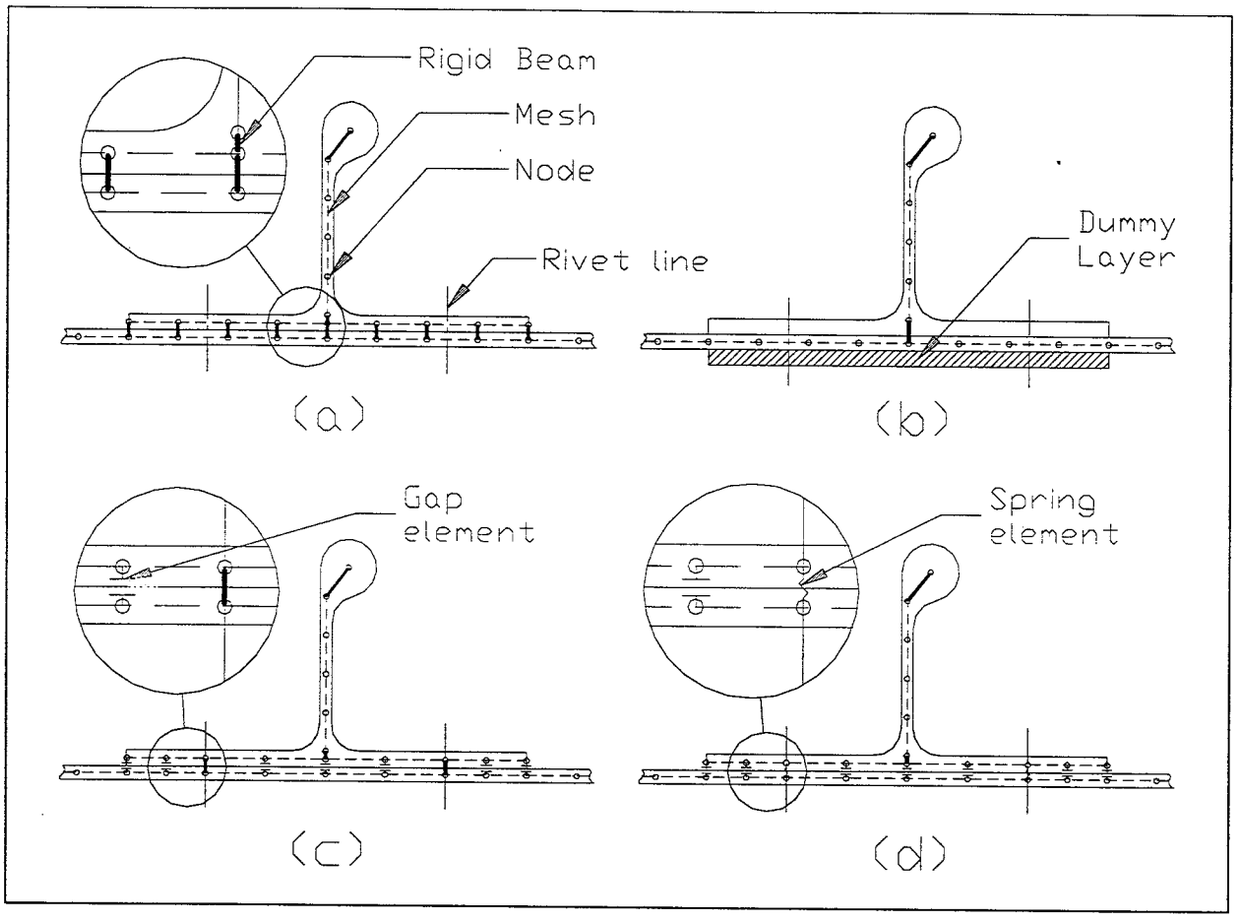


Figure 4: Methods of modelling the skin/stringer interface

Skin/Stringer Interface Modelling

Four different FE idealisations of the skin/stringer interface were examined. These different models are outlined schematically in Figure 4. In all four cases the bulb was connected to the web and the web to the flange by rigid beams (MPC type BEAM in ABAQUS). In method (a) the panel is assumed to act as an integral structure and the nodes on the skin and flange mid-surfaces were connected with rigid beams to account for the eccentricity between these mid-surfaces. Approach (b) also models the panel as an integral assembly but here a single layer of shells was used to model the skin and stringer flange. In this case the eccentricity was accounted for via the use of a "dummy layer" of low modulus material (similar to the model used by Skrna-Jakl *et. al* [4]) which effectively shifts the midplane of the skin/flange combination. The layer of shells was then modelled as a composite section. The remaining two approaches use rivet idealisations and allow separation of the skin and stringer flange to occur. The mesh was generated in such a way that adjacent nodes existed at the rivet locations. These nodes were connected with rigid beams in method (c). In method (d) a combination of spring elements was used to connect these nodes with one spring element representing the axial stiffness and two spring elements representing the shear stiffness of the rivet (the flexible joint element, JOINTC, was used to define the three spring elements at each rivet location). The contact conditions between the remaining nodes were represented using gap elements in both cases.

Mesh, Loads and Boundary Conditions

As mentioned in the previous section the mesh used in approaches (c) and (d) was slightly different to that used in (a) and (b). Both meshes are shown in Figure 5 (the mesh used in method (b) is identical to that used in (a) with the layer of shells representing the flange removed). It is worth noting here that the top and bottom rows of elements represent the 0.5" of material cast within the Cerrobend on either end and that the two outermost rows of shell elements represent the 0.5" of skin material constrained between the support bars at each edge. Modelling this material was essential to ensure that the overall stiffness of the FE model was representative of the corresponding experimentally observed stiffness.

The loading and boundary conditions applied to the models were exactly the same in all four cases. A uniform axial displacement was applied to one end of the panel with the displacements at the opposite end restrained in the X-direction. The nodes of the top and bottom rows of

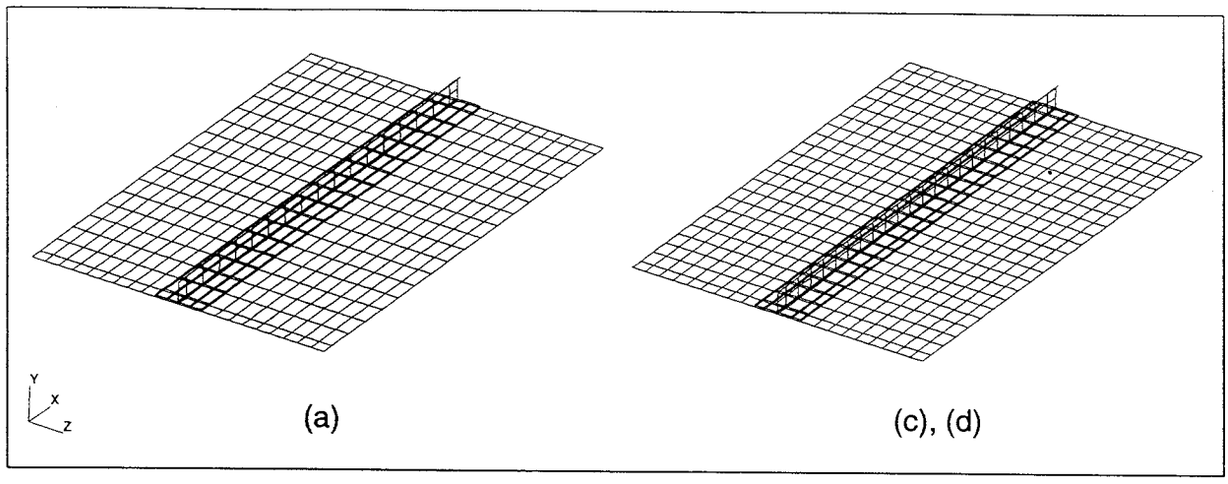


Figure 5: Meshes used in FE analysis of panel

elements (cast within Cerrobend) were restrained in the Y- and Z-directions and the nodes of the outermost rows of elements (between support bars) were restrained in the Y-direction.

Analysis Procedure

The buckling loads and corresponding mode shapes for each model were determined from an eigenvalue buckling analysis. The initial geometry was then seeded with an imperfection in the shape of the first buckling mode obtained from the eigenvalue buckling analysis. The maximum magnitude of this imperfection was 10% of the skin thickness. The postbuckling analysis was performed on the imperfect model using an arc-length solution technique (RIKS solution procedure in ABAQUS) and the analysis terminated when the end-shortening exceeded 0.12".

## Theoretical Analysis

The theoretical approach outlined here is primarily based on that presented by Bruhn[1] and ESDU[16]. The rivet pitch of the panel had been chosen to be sufficiently small so as to eliminate the possibility of inter-rivet buckling hence this mode was not considered.

For the panel under consideration the boundary conditions for the loaded and unloaded edges are known to be fully fixed. In an actual fuselage panel the boundary conditions for the loaded edges would be dependent on the support offered by the frame to the skin and stringer. The boundary conditions for the unloaded edges would be dependent on the support offered by the stringer to the skin. In both cases the exact nature of these support conditions is indeterminate and hence the boundaries are (conservatively) assumed to be simply-suppported. In our case, as we know these boundary conditions, the buckling and failure loads can be estimated more accurately than for an actual fuselage panel. Therefore the theoretical analysis will be presented for two separate cases; a least conservative case, Theory1, and a most conservative case, Theory2 (based on current practice). These two cases will demonstrate the range of conservatism associated with current techniques.

In the following sections the subscripts (sk) and (str) refer to the skin and stringer respectively. Figure 6 defines some of the parameters used for the theoretical analysis of the panel.

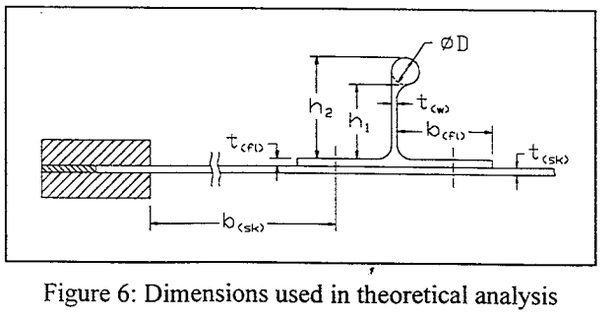


Figure 6: Dimensions used in theoretical analysis

Local Buckling

The stress in the skin at which local buckling occurs is given by:

$$f_{b(sk)} = \frac{k\pi^2 E_{t(sk)}}{12\left(1-\nu^2\right)}\left(\frac{t_{(sk)}}{b_{(sk)}}\right)^2 \qquad (2)$$

The skin is assumed to be simply supported along the rivet line and fully clamped along the remaining three edges for Theory1. For Theory2 the skin is assumed to be simply supported on all four edges. The buckling coefficient $k$, can be obtained from Figure C5.2 in Ref. 1 for each support case. $E_{t(sk)}$ is the tangent modulus of the skin material at $f_{b(sk)}$ (which is used to account for plasticity). Using a Ramberg-Osgood fit the tangent modulus at a stress $f$ is given by:

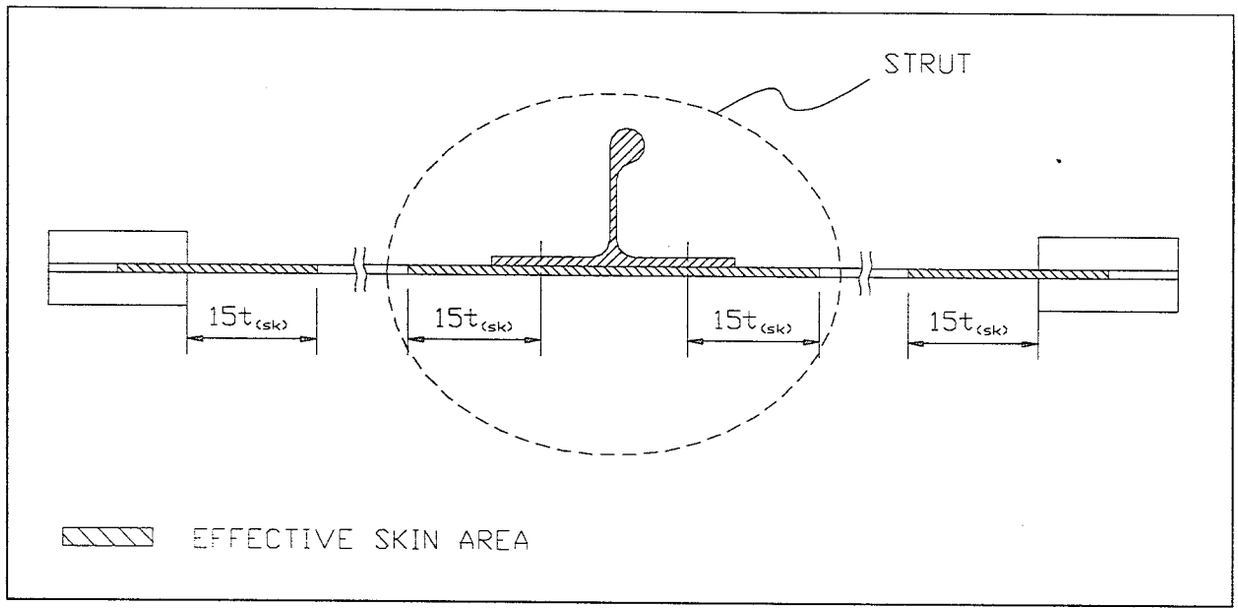


Figure 7: Effective postbuckled skin

$$E_t = E\left[1+\left(\frac{f}{f_n}\right)^{m-1}\right]^{-1} \tag{3}$$

where $E$, $m$ and $f_n$ are given in Table 1 for each material. Therefore the solution to equation 2 is iterative. The strain required to induce a stress of $f_{b(sk)}$ in the skin is then calculated as:

$$\varepsilon_{b(sk)} = \frac{1}{E_{(sk)}}\left[f_{b(sk)} + \frac{f_{n(sk)}}{m_{(sk)}}\left(\frac{f_{b(sk)}}{f_{n(sk)}}\right)^{m_{(sk)}}\right] \tag{4}$$

which is equal to the strain in the stringer. Hence the corresponding stress in the stringer $f_{b(str)}$ is determined from the following equation:

$$\varepsilon_{b(sk)} = \frac{1}{E_{(str)}}\left[f_{b(str)} + \frac{f_{n(str)}}{m_{(str)}}\left(\frac{f_{b(str)}}{f_{n(str)}}\right)^{m_{(str)}}\right] \tag{5}$$

the solution to which is also iterative. The local buckling load is then given by:

$$P_b = \left(f_{b(sk)}A_{(sk)}\right) + \left(f_{b(str)}A_{(str)}\right) \tag{6}$$

where $A_{(sk)}$ and $A_{(str)}$ are the cross-sectional areas of the skin and stringer respectively.

Stringer Crippling

In order to determine the failure load of the panel the crippling stresses of the stringer bulb, web and flanges must first be determined. These stresses are derived from the local buckling stresses of the stringer web and flanges. For the stringer flanges the local buckling stress is:

$$f_{b(fl)} = \frac{0.64\pi^2 E_{t(str)}}{12\left(1-\nu^2\right)}\left(\frac{t_{(fl)}}{b_{(fl)}}\right)^2 \tag{7}$$

Similarly the local buckling stress of the stringer web is given by:

$$f_{b(w)} = \frac{k\pi^2 E_{t(str)}}{12\left(1-\nu^2\right)}\left(\frac{t_{(w)}}{b_{(w)}}\right)^2 \tag{8}$$

where $k$ is dependant on edge support conditions. These in turn are dependent on the bulb size; if $D \geq 2t_{(w)}$ the bulb is assumed to offer simple support to the web in which case $k = 4$ and the web height, $b_{(w)} = h_1$. Otherwise the web and the bulb are assumed to act together as a flange giving $k = 0.64$ and $b_{(w)} = h_2$. The flange and web crippling stresses, $f_{cr}$ , are calculated from the corresponding local buckling stresses using the equation:

$$f_{cr} = \sqrt{f_b f_{cy(str)}} \tag{9}$$

where $f_{cy(str)}$ is given in Table 1. If $D \geq 2t_{(w)}$ the bulb crippling stress is:

$$f_{cr(bulb)} = 0.7 \times f_{cr(w)} \tag{10}$$

If $D < 2t_{(w)}$ the bulb crippling stress is equal to the web crippling stress (as the bulb and web act together as a flange).

Panel Failure

Panel failure was assumed to occur in a stringer-local-flexural mode. In the postbuckled regime the stringer, together with some effective skin, is assumed to act as a strut. This effective skin is the hatched area directly underneath the stringer in Figure 7. Failure of the strut occurs when the average stress in the stringer, $f_{av}$, reaches a level at which a pre-defined allowable stress, $f_{all}$, is induced in the most compressed fibre of the strut. The relationship between $f_{all}$ and $f_{av}$ is given by the Secant formula:

$$f_{all} = f_{av}\left[1+\frac{ey}{\rho^2}\sec\frac{l'}{2\rho}\sqrt{\frac{f_{av}}{E_{t(str)}}}\right] \qquad (11)$$

- $e$ is the eccentricity of the strut which is estimated from the greater of $0.05\rho^2/\sqrt{(y_p y_n)}$ and $0.001l$ where $\rho$ is the radius of gyration of the cross-section, $y_p$ and $y_n$ are the distances from the neutral axis to the extreme fibres either side of the axis and $l$ is the length of the strut (=16").
- $y$ is the distance from the neutral axis to the most compressed fibre (=$y_p$ or $y_n$)
- $l'$ is the equivalent length of the strut given by $l/\sqrt{c}$ where $c$=1 for a simply supported end condition (Theory2) and $c$=4 for a fully fixed end condition (Theory1).

An iterative solution is required to determine $f_{av}$ from equation 11. The allowable stress is taken to be the minimum of $f_{cr(bulb)}$ and $f_{cy(str)}$ on the bulb side and the minimum of $f_{cr(fl)}$ and $f_{cy(str)}$ on the flange side. Therefore the average stresses in the stringer corresponding to each allowable stress must be calculated. The lower of the average stresses gives the failure stress in the stringer, $f_{ult(str)}$, and the failure mode i.e. skin-side or bulb-side failure.

The stress in the effective skin at failure, $f_{ult(sk)}$, is obtained by calculating the strain in the stringer at failure and then, at this strain, determining the stress in the skin (as per equations 4 and 5). The stress in the remaining skin is $f_{b(sk)}$. Therefore the failure load of the panel is given by:

$$P_{ult} = A_{(str)}f_{ult(str)} + A_{(eff)}f_{ult(sk)} + \left(A_{(sk)} - A_{(eff)}\right)f_{b(sk)} \qquad (13)$$

where $A_{(eff)}$ is the total effective skin area (the entire hatched region of skin in Figure 7).

## Results and Discussion

Comparison of Experimental, FE and Theoretical Results

The experimental, finite element and theoretical buckling and failure loads together with the percentage error based on the experimental values are presented in Table 3. The discrepancies between the test data and the FE predictions using models (a) and (b) indicate the possible errors associated with analysing a riveted structure as an integral structure. This is reinforced by the accuracy of models (c) and (d) which allow separation of the skin and stringer flange to occur. Theory1 also provides accurate predictions of the buckling and failure loads whereas the more conservative Theory2 underestimates these loads significantly.

| | $P_b$ (lbf) | % error in $P_b$ | $P_{ult}$ (lbf) | % error in $P_{ult}$ |
|---|---|---|---|---|
| test | 8610 | ---- | 24299 | ---- |
| FE (a) | 10493 | 21.9 | 27169 | 11.8 |
| FE (b) | 10504 | 22.0 | 27153 | 11.7 |
| FE (c) | 8840 | 2.7 | 24610 | 1.3 |
| FE (d) | 8068 | -6.3 | 24109 | -0.8 |
| Theory1 | 8925 | 3.7 | 23950 | -1.4 |
| Theory2 | 6503 | -24.5 | 18337 | -24.5 |

Table 3: Experimental, FE and theoretical buckling and failure loads

All four FE models correctly predict the buckling mode of the panel, given by four half-wavelengths along the skin and one half-wavelength across the skin. The experimental and finite element load-deflection curves for the panel are shown in Figure 8. The significant differences between models (a) and (b) and models (c) and (d) can clearly be seen from this graph, again highlighting the importance of modelling the skin/stringer interface correctly. There is a noticeable difference in post-failure stiffness of the integral FE models and the riveted FE models. This is attributable to the different failure modes predicted by these models, shown in Figure 9. The integral FE models exhibit a skin-side failure mode resulting in a gradual reduction of stiffness in the post-failure regime whereas the riveted FE models exhibit bulb-side failure which causes a sharp reduction in stiffness shortly after failure. This bulb-side failure mode corresponds to the actual failure mode, as shown in Figure 10. The behaviour of models (a) and (b) is almost identical and therefore either method could be used to model an integral (e.g. extruded or machined) panel. There are slight differences between the load-deflection characteristics of models (c) and (d) due to the increased flexibility generated by idealising the rivets using spring elements as opposed to rigid beams. The underestimation of the buckling load by model (d) indicates an error in the stiffness of the spring elements used to represent the rivets.

The stiffness of the panel in both the pre and postbuckling regimes predicted by all four FE models was considerably higher than the experimentally observed values (see Figure 8). This was shown to be due to the

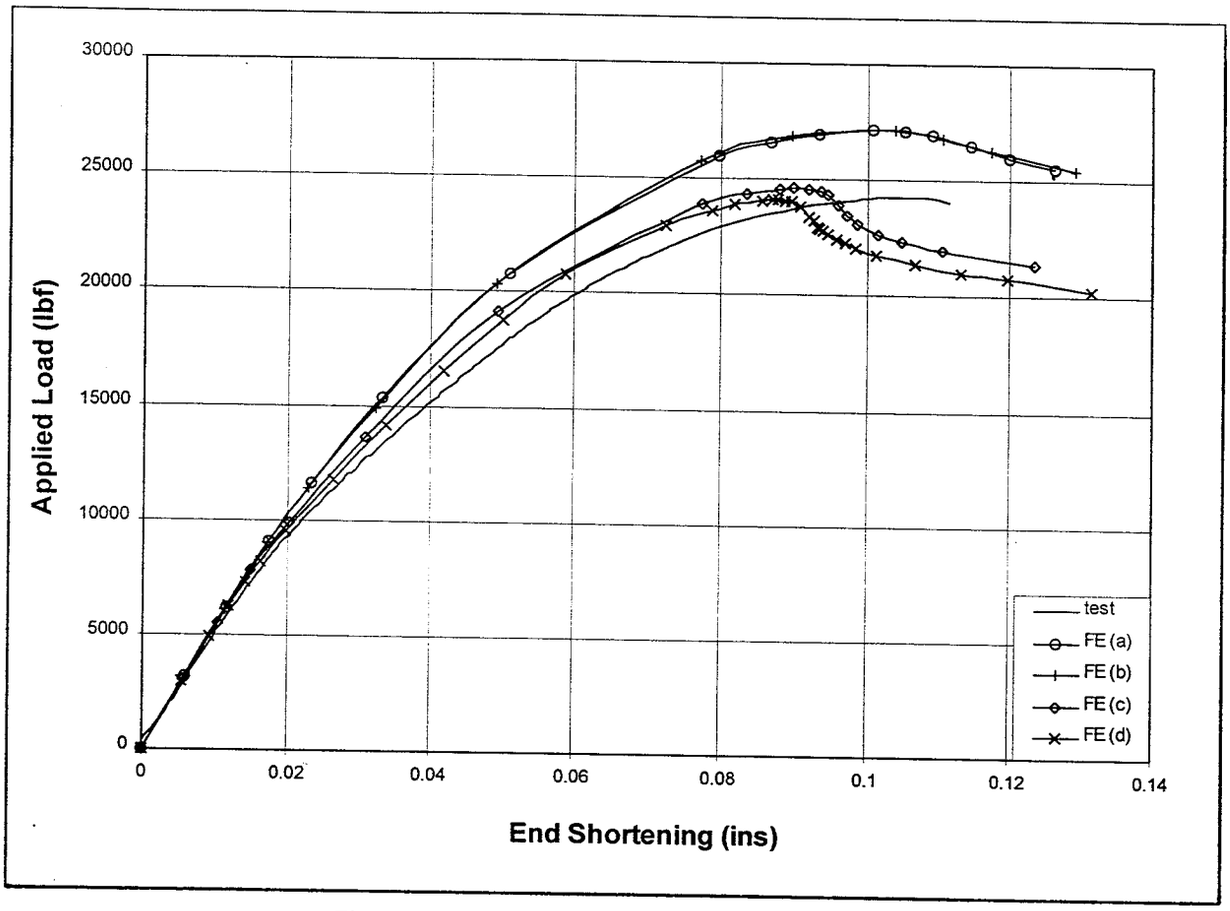


Figure 8: FE and experimental load-deflection curves

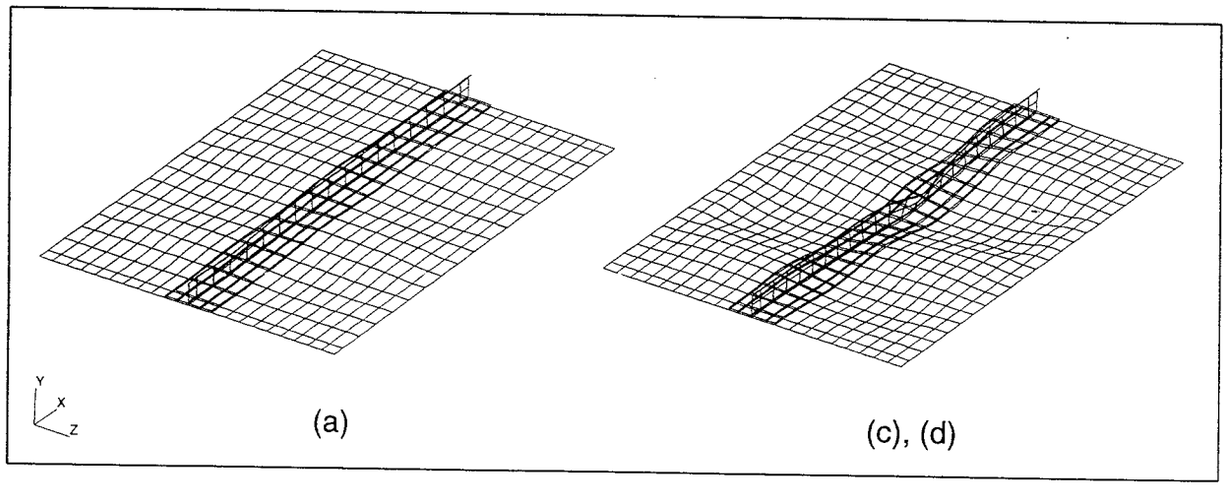


Figure 9: Finite element failure modes

tendency of the skin, as buckling initiated, to separate the support bars. This separation of the support bars effectively increases the amount of buckled skin, thus reduces the amount of effective skin and decreases the panel stiffness. The large differences between the experimental and FE end shortening at failure are as a direct result of the corresponding stiffness discrepancies.

Details of the FE postbuckling solutions are given in Table 4. The large run-times of models (c) and (d) are due to the time consuming severe discontinuity iterations associated with contact analysis. Method (b) is clearly more efficient for the FE analysis of integral panels. Method (c) is the more accurate of the two riveted models although it is felt that, using more precise spring

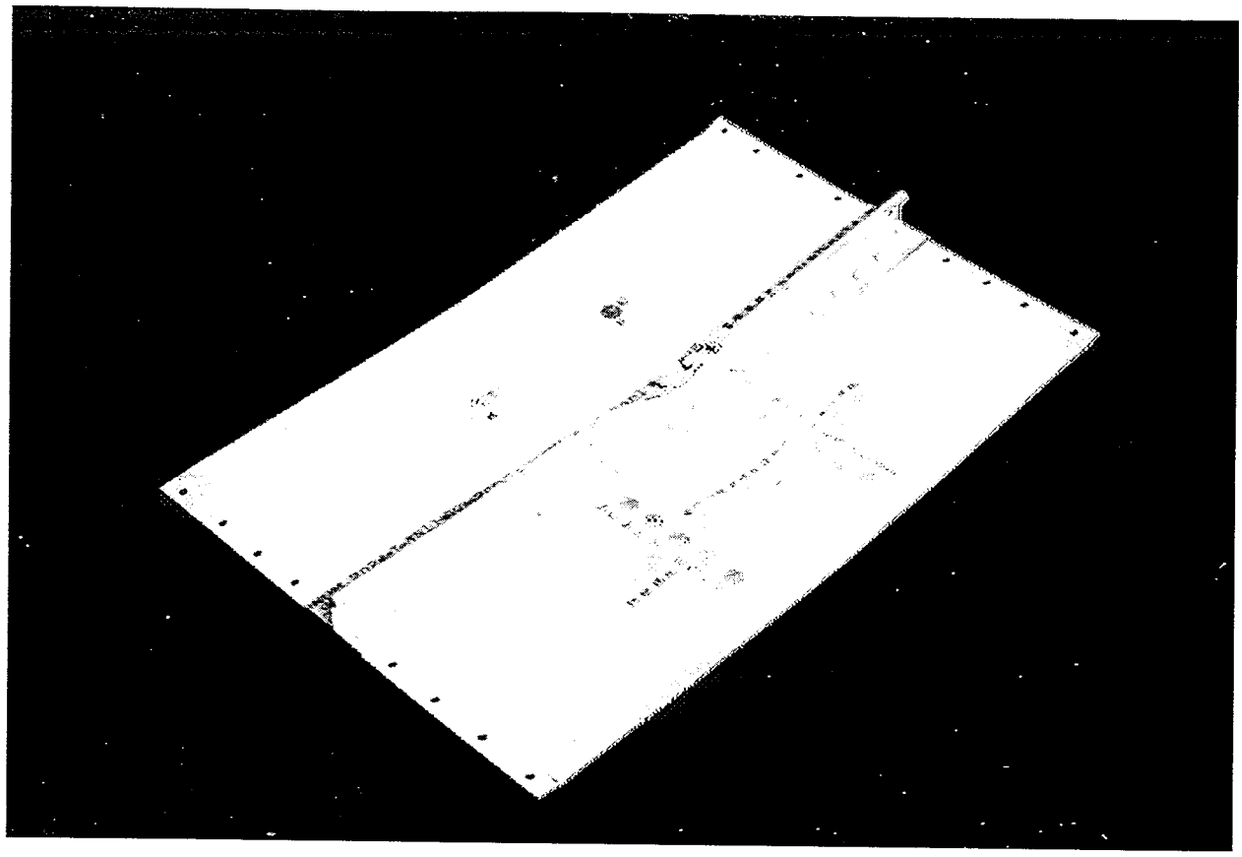

Figure 10: Failure mode of test panel

stiffnesses to model the rivets, method (d) may be more representative of the actual structure. However the run-time associated with method (d) is almost double that of method (c), hence the latter is clearly the most efficient modelling technique for the postbuckling analysis of riveted fuselage panels. It is also worth noting that the number of iterations required to reach the failure load of the panel is significantly lower than the number of iterations taken to exceed the prescribed displacement. From a design point of view the post-failure behaviour of the panel is unimportant hence the extra iterations taken to exceed this prescribed displacement are unnecessary. Thus, for method (c), the number of iterations could be halved resulting in much lower run-times.

The correlation between Theory1 predictions and test results was excellent. The more conservative estimates, obtained using Theory2 are approximately 25% over-conservative. If the panel considered were part of an actual fuselage panel the boundary conditions at the loaded and unloaded edges would be more flexible than the fully clamped support conditions of the test panel. Hence the FE and experimental buckling and failure loads reported in Table 1 would be somewhat closer to the values predicted by Theory 2. Therefore 25% is the limiting value of conservatism associated with current analysis techniques. A test program is currently underway to estimate more accurately the degree of conservatism associated with these analytical techniques.

| | Total No. of Increments | Total Run-Time[(a)] | No. of Increments to Failure |
|---|---|---|---|
| FE (a) | 15 | 1.33 hrs | 10 |
| FE (b) | 12 | 0.83 hrs | 9 |
| FE (c) | 20 | 5.67 hrs | 10 |
| FE (d) | 42 | 10.83 hrs | 16 |

(a) Based on CPU times using a Silicon Graphics Indigo workstation with 64MB of RAM.

Table 4: Solution details of postbuckling analyses

Potential Weight Savings

The test panel was redesigned using finite element method (c), Theory1 and Theory2 with a view to converting the conservatism outlined above to a possible weight saving. MIL-HDBK material properties were used and the overall dimensions of the panel were kept constant, i.e. 11.24"×17". The stringer width, rivet pitch and rivet spacing were also kept constant. The buckling and ultimate design loads were 8000lbf and 24000lbf respectively. The resulting panel geometries are given in Table 5 together with the buckling loads, failure loads and panel weight.

The weight penalty given in Table 5 is the percentage increase in panel weight incurred by

designing the panel using either Theory1 or Theory2. Therefore, using the above reasoning, if the panel considered were part of an actual fuselage panel a weight reduction of 5-12% could be achieved by employing the finite element method over conventional analytical techniques.

| | FE (c) | Theory1 | Theory2 |
|---|---|---|---|
| $t_{(sk)}$ (ins) | 0.053 | 0.057 | 0.064 |
| $t_{(fl)}$ (ins) | 0.094 | 0.094 | 0.090 |
| $t_{(w)}$ (ins) | 0.094 | 0.094 | 0.090 |
| D (ins) | 0.250 | 0.250 | 0.250 |
| $h_2$ (ins) | 1.206 | 1.206 | 1.206 |
| $P_b$ (lbf) | 8155 | 8220 | 8082 |
| $P_{ult}$ (lbf) | 24590 | 24170 | 24272 |
| Weight[a] | 1.5625lbs | 1.6397lbs | 1.7568lbs |
| Weight Penalty | ------ | 4.9% | 12.4% |

(a) The density of both aluminium alloys was taken to be 0.101lbs/in$^3$

Table 5: Details of redesigned panels

## Conclusions

This paper has presented a finite element methodology for the compressive postbuckling analysis of a flat stiffened riveted panel. Several different modelling techniques were investigated and the resulting structural response compared to both experimental and theoretical data.

- Of the elements considered the second-order small strain thin shell S8R5 was the most reliable for buckling analysis.
- It has been shown that a riveted panel cannot be modelled as an integral structure. The separation of the skin and stringer flange can result in a significant reduction of the buckling and failure loads of the structure.
- Correlation between the riveted FE models and the corresponding test data was very good. FE predictions of the buckling and failure loads were within 2.5% of the experimental values.
- For the panel considered, current analysis techniques underestimated the buckling and failure loads by approximately 25%, although this error would not be as pronounced in the case of an actual fuselage panel.
- The potential weight savings achievable by using the FE technique presented herein as opposed to conventional analytical techniques has been estimated to be between 5% and 12%.

## References

1. Bruhn, E.F., "Analysis and Design of Flight Vehicle Structures", Tri-State Offset Company, USA
2. Meyer-Piening, H. and Anderegg, R., "Buckling and Postbuckling Investigations of Imperfect Curved Stringer-Stiffened Composite Shells. Part A: Experimental Investigation and Effective Width Evaluation", Thin Walled Structures, 1995, Vol.23, No.1-4, pp.323-338
3. Zdunek, A., "Shear Buckling of a Cylindrical Carbonfibre Reinforced Panel: Analyses with ABAQUS- and STRIPE-codes", Aeronautical Research Institute of Sweden, 1994, FFA TN 1993-10
4. Skrna-Jakl, I., Stiftinger, M. and Rammerstorfer, F., "Numerical Investigations of an Imperfect Stringer-Stiffened Composite Wing Torsion Box - An Analysis Concept", Composites, 1996, Vol.27B, No.1, pp.59-69
5. Scott, M., "Non-linear Finite Element Modelling of an Integrally Stiffened Composite Panel", Composite Structures, 1994, Vol.29, No.2, pp.213-218
6. Falzon, B. and Steven, G., "Buckling Mode Transition in Hat-Stiffened Composite Panels Loaded in Uniaxial Compression", Composite Structures, 1997, Vol.37, No.2, pp.253-267
7. Jiang, W., Bao, G. and Roberts, J., "Finite Element Modeling of Stiffened and Unstiffened Orthotropic Plates", Computers & Structures, 1997, Vol.63, No.1, pp.105-117
8. Percy, W. and Fields, R., "Buckling Analysis and Test Correlation of Hat Stiffened Panels for Hypersonic Vehicles", AIAA 90-5219, presented at the AIAA Second International Aerospace Planes Conference, Orlando, Florida, Oct. 29-31, 1990
9. Ko, W. and Jackson, R., "Compressive Buckling Analysis of Hat-Stiffened Panel", NASA TM-4310, 1991
10. Ko, W. and Jackson, R., "Shear Buckling Analysis of a Hat-Stiffened Panel", NASA TM-4644, 1994
11. Shanmugam, N. and Arockiasamy, M., "Local Buckling of Stiffened Plates in Offshore Structures", Journal of Constructional Steel Research, 1996, Vol.38, No.1, pp.41-59
12. Hibbitt Karlsson & Sorensen Inc., ABAQUS/Standard User's Manual Version 5.6, 1996
13. Department of Defense, Washington, DC, MIL-HDBK-5G, Nov.1, 1994
14. Rothwell, A., "An Experimental Investigation of the Post-buckled Efficiency of Z-Section Stringer-Skin Panels", Aeronautical Journal, 1981, Vol.85, No.840, pp.29-33
15. Hibbitt Karlsson & Sorensen Inc., ABAQUS Theory Manual Version 5.6, 1996
16. ESDU, "The Strength of Struts", Engineering Sciences Data Item 01.01.01, Structures Sub-series, Vol.11, 1990